Arginine 177 Is Involved in Mn(II) Binding by Manganese Peroxidase†

Maarten D. Sollewijn Gelpke, Pierre Moënne-Loccoz, and Michael H. Gold*

Department of Biochemistry and Molecular Biology, Oregon Graduate Institute of Science and Technology, Beaverton, Oregon 97006-8921

Received April 26, 1999; Revised Manuscript Received July 15, 1999

ABSTRACT: Site-directed mutations R177A and R177K in the gene encoding manganese peroxidase isozyme 1 (*mnp1*) from *Phanerochaete chrysosporium* were generated. The mutant enzymes were expressed in *P. chrysosporium* during primary metabolic growth under the control of the glyceraldehyde-3-phosphate dehydrogenase gene promoter, purified to homogeneity, and characterized by spectroscopic and kinetic methods. The UV−vis spectra of the ferric and oxidized states and resonance Raman spectra of the ferric state were similar to those of the wild-type enzyme, indicating that the heme environment was not significantly affected by the mutations at Arg177. Apparent K_m values for Mn^{II} were ∼20-fold greater for the R177A and R177K MnPs than for wild-type MnP. However, the apparent K_m values for the substrates, H_2O_2 and ferrocyanide, and the k_{cat} values for Mn^{II} and ferrocyanide oxidation were similar to those of the wild-type enzyme. The second-order rate constants for compound I (MnPI) reduction of the mutant MnPs by Mn^{II} were ∼10-fold lower than for wild-type MnP. In addition, the K_D values calculated from the first-order plots of MnP compound II (MnPII) reduction by Mn^{II} for the mutant enzymes were ∼22-fold greater than for wild-type MnP. In contrast, the first-order rate constants for MnPII reduction by Mn^{II} were similar for the mutant and wild-type MnPs. Furthermore, second-order rate constants for the wild-type and mutant enzymes for MnPI formation, for MnPI reduction by bromide, and for MnPI and MnPII reduction by ferrocyanide were not significantly changed. These results indicate that both the R177A and R177K mutations specifically affect the binding of Mn, whereas the rate of electron transfer from Mn^{II} to the oxidized heme apparently is not affected.

White-rot basidiomycete fungi are capable of degrading the plant cell wall polymer, lignin (*1*−*3*), and a variety of aromatic pollutants (*4*−*7*). When cultured under lignolytic conditions, the best-studied lignin-degrading fungus, *Phanerochaete chrysosporium*, secretes two families of extracellular peroxidases, lignin peroxidase (LiP)[1] and manganese peroxidase (MnP), which, along with an H_2O_2-generating system, constitute the major enzymatic components of its extracellular lignin-degrading system (*1*, *2*, *8*−*10*). Both LiP and MnP are able to depolymerize lignin in vitro (*10*−*12*), and MnP activity has been found in essentially all lignin-degrading fungi that have been examined (*13*−*16*).

MnP from *P. chrysosporium* has been purified to homogeneity and characterized (*3*, *16*−*19*). In addition, genomic and cDNA sequences of *P. chrysosporium* MnP isozymes *mnp1*, *mnp2*, and *mnp3* have been reported (*20*−*25*). X-ray crystallographic studies and DNA sequence comparisons indicate that the heme environment of MnP is similar to that of other plant and fungal peroxidases (*22*, *26*−*30*). Spectroscopic studies have revealed that the heme iron of the native enzyme is in the ferric, high-spin, pentacoordinate state and is ligated to the proximal histidine (*26*, *31*, *32*). Kinetic and spectroscopic characterization of the oxidized intermediates, MnP compounds I and II (MnPI and MnPII), indicates that the catalytic cycle of MnP is similar to that of horseradish peroxidase and LiP. However, MnP is unique in its ability to oxidize Mn^{II} to Mn^{III} (*3*, *18*, *19*, *33*−*36*). The reactions involved in the MnP catalytic cycle are

$$MnP + H_2O_2 \rightarrow MnPI + H_2O$$

$$MnPI + Mn^{II} \rightarrow MnPII + Mn^{III}$$

$$MnPII + Mn^{II} \rightarrow MnP + Mn^{III} + H_2O$$

The enzyme-generated Mn^{III} is stabilized by organic acid chelators such as oxalate, which is secreted by the fungus (*19*, *37*, *38*). The Mn^{III}−organic acid complex, in turn, oxidizes phenolic substrates such as lignin substructures (*39*) and aromatic pollutants (*6*, *40*, *41*).

Previously, we developed a homologous expression system for MnP isozyme 1 (*42*) in which the *P. chrysosporium* glyceraldehyde-3-phosphate dehydrogenase (*gpd*) gene promoter is used to drive expression of the *mnp1* gene during primary metabolic growth when endogenous MnP is not expressed. This expression system has been used to produce

† This research was supported by Grant MCB9808430 from the National Science Foundation (to M.H.G.) and Grant GM34468 from the National Institutes of Health (to T. M. Loehr).

* To whom correspondence should be addressed: Department of Biochemistry and Molecular Biology, Oregon Graduate Institute of Science and Technology, 20000 N.W. Walker Rd., Beaverton, OR 97006-8921. Telephone: (503) 748-1076. Fax: (503) 748-1464. E-mail: mgold@bmb.ogi.edu.

[1] Abbreviations: DMP, 2,6-dimethoxyphenol; gpd, glyceraldehyde-3-phosphate dehydrogenase; HCHN, high-carbon and high-nitrogen; LiP, lignin peroxidase; MnP, manganese peroxidase; MnPI, MnP compound I; MnPII, MnP compound II; RR, resonance Raman; SDS−PAGE, sodium dodecyl sulfate−polyacrylamide gel electrophoresis; wtMnP, wild-type MnP.

10.1021/bi990943c CCC: $18.00
Published on Web 08/12/1999

and characterize mutants of Mn binding site ligands and of the heme cavity residue Phe190 (*43*−*45*).

The MnP crystal structure (*26*) contains a unique Mn binding site involved in the oxidation of Mn^{II}. In this site, the single Mn atom is hexacoordinate, with carboxylate ligands from the heme propionate 6 and from amino acids Glu35, Glu39, and Asp179. The final two ligands are waters. When Glu35, Glu39, and Asp179 are mutated to their respective amides, a significant effect on the kinetics of Mn^{II} oxidation is observed, confirming that these residues are Mn binding ligands and that the proposed Mn binding site is the productive site (*43*, *44*, *46*). In addition to these amino acid ligands, Arg177 also appears to be a component of the Mn binding site (*26*). The crystal structure shows that Arg177 forms a salt bridge with Glu35, orienting this ligand for efficient Mn binding (*26*). In this study, we investigate the role of Arg177 in Mn^{II} oxidation using spectroscopic and kinetic analyses of two Arg177 mutants.

MATERIALS AND METHODS

Organisms. P. chrysosporium wild-type strain OGC101, auxotrophic strain OGC107-1 (Ade1), and prototrophic transformants were maintained as described previously (*47*). *Escherichia coli* DH5α was used for subcloning plasmids.

Construction of Transformation Plasmids. The R177A and R177K site-directed mutations were introduced into the plasmid pGM1 (*43*), which contains 1.1 kb of the *gpd* promoter fused to the *P. chrysosporium mnp1* gene at the translation start site. The PCR-based Quikchange (Stratagene) protocol was used for site-directed mutagenesis. A forward and reverse primer for each mutation was designed to change the CGC codon (Arg) to a GCC (Ala) or an AAG (Lys) codon. After the mutagenesis reactions, two plasmids, pGM11 and pGM12, containing the R177A and R177K mutations, respectively, were isolated, and the mutations were confirmed by sequencing. Subsequently, the *Xba*I−*Eco*RI fragments of pGM11 and pGM12, containing the *gpd* promoter and the mutated *mnp1* genes, were subcloned into pOGI18 (*48*), a *P. chrysosporium* transformation plasmid, containing the *Schizophyllum commune ade*5 gene as a selectable marker. This generated the *P. chrysosporium* transformation plasmids pAGM11 and pAGM12 for the R177A and R177K mutations, respectively. The *mnp1* coding sequences of pAGM11 and pAGM12, including the mutations, were verified by sequencing.

Transformation of P. chrysosporium. Protoplasts of the Ade^- strain OGC107-1 were transformed as described previously (*47*), using 1 μg of linearized pAGM11 or pAGM12 as the transforming DNA. Prototrophic transformants were transferred to minimal medium slants to confirm adenine prototrophy and assayed for MnP activity using the *o*-anisidine plate assay described previously (*42*). Transformants exhibiting the highest activity on plates were purified by fruiting as described previously (*47*, *49*), and the progeny were rescreened for MnP activity by the plate assay. The purified transformants with the highest MnP activity, AGM11 and AGM12, were selected for analysis.

Production and Purification of the MnP Mutant Proteins. Cultures of the selected transformants were maintained on slants and grown in liquid culture from conidial inocula (*42*). The MnP mutant proteins were purified from the extracellular medium of high-carbon and high-nitrogen (HCHN) liquid shake cultures, grown for 3 days at 28 °C (*42*). For each mutant protein, 14 1-L HCHN shake cultures in 2-L flasks were filtered, and the extracellular fluid was pooled and concentrated by ultrafiltration. Subsequently, variant proteins were purified by Phenyl-Sepharose hydrophobic interaction, Blue Agarose affinity, and Mono Q anionic exchange column chromatography as described previously (*44*). Wild-type MnP was produced and isolated as described previously (*17*, *36*).

SDS−*PAGE Analysis.* Sodium dodecyl sulfate−polyacrylamide gel electrophoresis (SDS−PAGE) was performed using a 12% Tris-glycine gel system (*50*) and a Miniprotean II apparatus (Bio-Rad), and gels were stained with Coomassie blue.

Enzyme Assays and Spectroscopic Procedures. Electronic absorption spectra of the various oxidation states of the MnP enzymes and steady-state kinetic assays were recorded and conducted, respectively, at room temperature using a Shimadzu UV-260 spectrophotometer. The extent of Mn^{II} oxidation by MnP was measured by following the formation of the Mn^{III}−malonate complex at 270 nm ($\epsilon_{270} = 11.6\ mM^{-1}\ cm^{-1}$) (*19*). The extent of oxidation of ferrocyanide was measured at 420 nm ($\epsilon_{420} = 1\ mM^{-1}\ cm^{-1}$) as described previously (*51*).

MnPI was prepared by mixing 1 equiv of H_2O_2 with the native enzyme in 20 mM potassium phosphate buffer (pH 6.0). MnPII was prepared by the successive addition of 1 equiv of ferrocyanide and 1 equiv of H_2O_2 to the native enzyme in 20 mM potassium malonate buffer (pH 4.5). Enzyme concentrations were determined at 407 nm ($\epsilon_{407} = 129\ mM^{-1}\ cm^{-1}$) (*17*).

Kinetic Analysis. Apparent K_m and k_{cat} values for Mn^{II} and H_2O_2 were calculated from double-reciprocal plots of the initial rate of Mn^{III}−malonate formation versus varying Mn^{II} or H_2O_2 concentrations. A double-reciprocal plot of the initial rate of ferricyanide formation versus substrate concentration was used to calculate the apparent K_m and k_{cat} values for ferrocyanide. Reaction mixtures (1 mL) contained H_2O_2 (0.1 mM), 0.5 μg of MnP for Mn^{II} oxidation or 5 μg of MnP for ferrocyanide oxidation, and varying concentrations of $MnSO_4$ (0.02−10 mM) or ferrocyanide (1−15 mM) in 50 mM potassium malonate (pH 4.5) (ionic strength $\mu = 0.1$ M, adjusted with K_2SO_4). To determine apparent K_m values for H_2O_2, reactions were conducted in 5 mM $MnSO_4$.

Transient-state kinetic measurements were taken at 25 °C using an Applied Photophysics stopped-flow reaction analyzer (SX.18MV) with sequential mixing and a diode array detector for rapid scanning spectroscopy. The extent of MnPI formation was measured at 397 nm, the isosbestic point between compounds I and II. Native enzyme (2 μM) in 50 mM potassium malonate (pH 4.5) (ionic strength $\mu = 0.1$ M, adjusted with K_2SO_4) was mixed with a 10−50-fold excess of H_2O_2 in the same buffer. For the reduction of MnPI, this oxidized state was prepared by premixing 4 μM enzyme in H_2O with 1 equiv of H_2O_2. The reaction mixture was incubated for 4 s, and MnPI formation was confirmed by rapid scanning. Subsequently, Mn^{II} in 100 mM potassium malonate (pH 4.5), ferrocyanide, or 2,6-dimethoxyphenol (DMP) in 40 mM potassium malonate (pH 4.5), or bromide in 40 mM potassium succinate (pH 3.0) was added in a ≥10-fold molar excess. The extent of reduction of MnPI by Mn^{II} was measured at 417 nm, the isosbestic point between MnPII

and native MnP. The two-step reduction of MnPI by ferrocyanide or DMP was assessed at 420 nm, the absorption maximum of MnPII. This two-phase reduction of MnPI started with the rapid reduction of MnPI followed by the slow reduction of MnPII in a single combined experiment. The direct two-electron reduction of MnPI to the native enzyme by bromide was followed at 407 nm (*52*). The reduction of MnPII by Mn^{II} was assessed at 407 nm, the Soret maximum of the native enzyme. MnPII was prepared by premixing 4 μM enzyme and 1 equiv of ferrocyanide in 50 mM potassium malonate (pH 4.5) with 1 equiv of H_2O_2 in the same buffer. This mixture was incubated for 5 s, and the formation of MnPII was confirmed by rapid scanning spectroscopy. Subsequently, MnPII was mixed with 0.5−10 mM Mn^{II} in the same buffer. All kinetic traces exhibited single-exponential character from which pseudo-first-order rate constants were calculated. Typically, five or six substrate concentrations were used in triplicate measurements.

Resonance Raman Spectroscopy. Resonance Raman (RR) spectra were obtained on a custom spectrograph consisting of a McPherson (Acton, MA) model 2061/207 monochromator operated at a focal length of 0.67 m and a Princeton Instruments (Trenton, NJ) LN1100 CCD detector with a model ST-130 controller. Laser excitation was from Coherent (Santa Clara, CA) Innova 302 krypton (413.1 nm) and Innova 90-6 argon (514.5 nm) lasers. The laser lines were filtered through Applied Photophysics (Leatherhead, U.K.) prism monochromators to remove plasma emissions. The incident laser powers at the sample were ~20 (413.1 nm) and ~50 mW (514.5 nm). Spectra were collected in a 90°-scattering geometry from solution samples contained in glass capillary tubes at room temperature. Rayleigh scattering was attenuated by the use of Kaiser Optical (Ann Arbor, MI) super-notch filters. The spectral resolution was set to ~3.0 cm^{-1}. Indene and CCl_4 served as frequency and polarization standards, respectively. Optical absorption spectra of the Raman samples were obtained on a Perkin-Elmer Lambda 9 spectrophotometer to monitor sample integrity before and after laser illumination. Samples contained 100 μM MnP in 20 mM phosphate buffer (pH 6.0). Data were calibrated and analyzed with GRAMS/386 spectroscopic software (Galactic Industries Corp., Salem, NH).

Chemicals. Phenyl-Sepharose CL-4B, Cibacron Blue 3GA Agarose, potassium ferrocyanide, and H_2O_2 (30% solution) were obtained from Sigma. DMP was obtained from Aldrich and purified by silica gel column chromatography (the solvent being hexane/ethyl acetate) before use. All other chemicals were reagent grade. Solutions used for kinetic assays were prepared with HPLC-grade water obtained from Aldrich.

RESULTS

Expression and Purification of the Mutant Enzymes. The *mnp1* coding sequences, including the mutations, of the *P. chrysosporium* transformation plasmids pAGM11 and pAGM12 were verified by DNA sequencing. Transformation of the Ade^- strain (OGC107-1) with linearized pAGM11 or pAGM12 resulted in the isolation of multiple transformants which exhibited MnP activity on the plate assay. For each mutant, five of these transformants were selected and purified by fruiting (*47*, *49*, *53*), and the colonies from single basidiospores were rescreened for MnP activity. From the purified isolates with MnP activity, one isolate of each mutation was selected to obtain the strains AGM11 (R177A) and AGM12 (R177K). These transformant strains expressed extracellular recombinant MnP enzyme when grown in HCHN shake cultures at 28 °C for 3 days, whereas endogenous MnP is not expressed under these conditions (*42*). The mutant MnPs were purified to homogeneity as determined by SDS−PAGE. The molecular masses of the mutant MnPs (46 kDa) were identical to those of recombinant wild-type MnP (rMnP) and wild-type MnP (wtMnP) (data not shown). The yields of expressed mutant enzymes were comparable to those of rMnP (*42*). Typically, mutant enzymes were purified to R_z values of >5.

Table 1: Absorbance Maxima of Native and Oxidized Intermediates of Wild-Type and Mutant MnPs[a]

enzyme	native (nm)	compound I (nm)	compound II (nm)
wtMnP	407, 503, 637	403, 558, 649	420, 528, 555
R177A	407, 502, 638	400, 557, 648	420, 527, 555
R177K	407, 500, 639	400, 558, 648	420, 528, 556

[a] MnP compounds I and II were prepared as described in the text.

Spectral Properties of the MnP Mutant Enzymes. The optical absorption spectra of the native and oxidized intermediates, compounds I and II, for each of the MnP mutant enzymes were essentially identical to those of the wild-type enzyme (Table 1), suggesting the substitution of Ala or Lys for Arg177 does not significantly alter the heme environment of the protein.

Resonance Raman Spectroscopy. The high-frequency (~1300−1700 cm^{-1}) RR spectral regions that are characteristic of heme coordination and spin state are shown in panels A and B of Figure 1 for Soret band (413.1 nm) and Q-band (514.5 nm) excitation, respectively. The relative intensities of the ν^3 and ν^{10} modes at 1482/1492 and 1612/1628 cm^{-1}, respectively, are consistent with a mixture of 6cHS and 5cHS heme species in wtMnP. The RR spectrum of wtMnP is identical to that described previously (*44*). The RR spectra of the R177A and R177K mutant enzymes are essentially identical to that of the wtMnP enzyme. Only minor changes in intensities, but no frequency shifts, can be detected in the heme vibrational spectra. This suggests that the R177A and R177K mutations do not result in any significant perturbation of the heme moiety. The changes in the relative intensities of the ν^3 and ν^{10} bands for the mutants compared to those of wtMnP suggest that a slightly greater portion of the hemes in the mutant protein may be in the 5cHS state.

Steady-State Kinetics. Under steady-state conditions, linear double-reciprocal plots were obtained over a range of Mn^{II}, ferrocyanide, and H_2O_2 concentrations in 50 mM potassium malonate (pH 4.5) (ionic strength μ = 0.1 M, adjusted with K_2SO_4) for the mutant and wtMnP enyzmes. The apparent K_m values for Mn^{II}, ferrocyanide, and H_2O_2 and the apparent k_{cat} values for the Mn^{II} and ferrocyanide oxidation reactions are listed in Tables 2 and 3, together with the k_{cat}/K_m ratios. The apparent K_m and k_{cat} values of the Mn binding site mutant E35Q (*44*) are included for comparison. The apparent K_m values for H_2O_2 and ferrocyanide, ~50 μM and ~20 mM, respectively, are similar for the wtMnP and the Arg177 mutant enzymes. Likewise, the k_{cat} values for Mn^{II} and

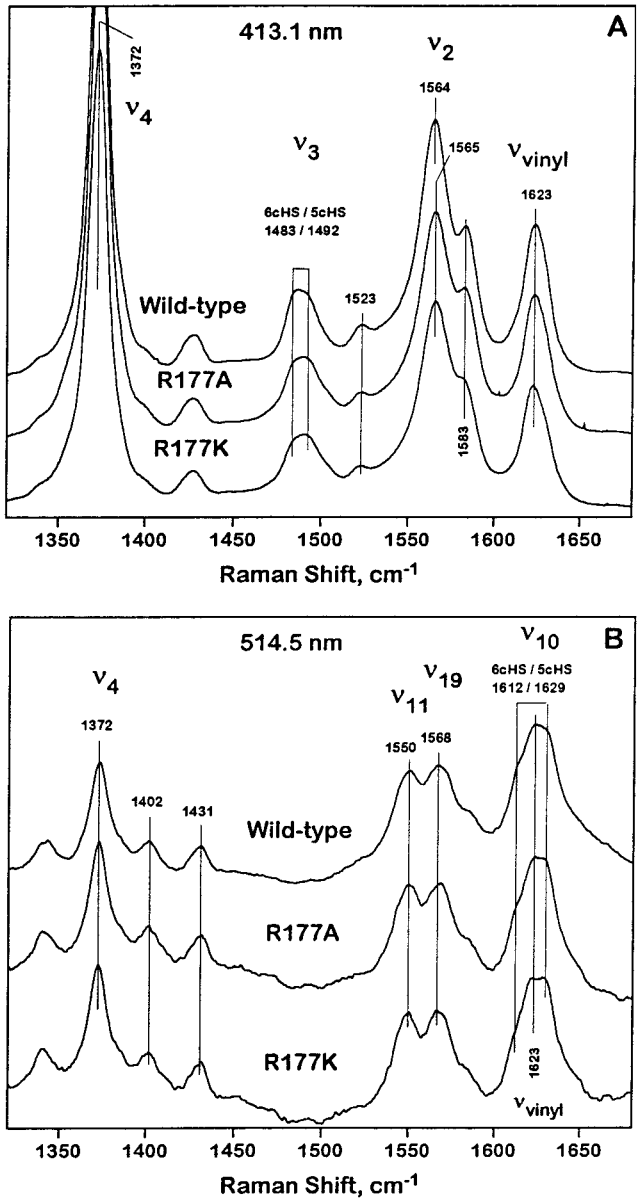

FIGURE 1: Resonance Raman spectra of the wild-type and mutant enzymes R177A and R177K (~100 μM) in 20 mM sodium phosphate (pH 6.0). Resonance Raman spectra of MnP enzymes were obtained with (A) Soret excitation (413.1 nm, 20 mW, 90° scattering geometry, and ambient temperature) and (B) Q-band excitation (514.5 nm, 50 mW, 90° scattering geometry, and ambient temperature). Frequencies and assignments for selected heme bands are shown. Polarization data also were collected to support the assignments.

ferrocyanide oxidation, 200−300 and ~40 s^{-1}, respectively, are similar for wtMnP and the Arg177 mutant enzymes. In contrast, the apparent K_m values for Mn^{II} for the R177A and R177K variants are ~20-fold higher than for wtMnP.

Formation of MnP Compound I. Rates of MnPI formation were determined in 50 mM potassium malonate (pH 4.5). We previously demonstrated that the rate of MnPI formation was not affected by the type or concentration of the organic acid chelator (*38*). The formation of MnPI was measured at 397 nm, and kinetic traces exhibited exponential character from which pseudo-first-order rate constants (k_{1obs}) were calculated. The k_{1obs} constants were linearly proportional to H_2O_2 concentrations at a 10−50-fold excess (data not shown). The second-order rate constants (k_{1app}) for MnPI formation were similar for wtMnP and the R177A and R177K mutant proteins (Table 4).

Table 2: Steady-State Kinetic Parameters for Wild-Type and Mutant MnPs[a]

	Mn^{II}			H_2O_2		
enzyme	K_m (μM)	k_{cat} (s^{-1})	k_{cat}/K_m (M^{-1} s^{-1})	K_m (μM)	k_{cat} (s^{-1})	k_{cat}/K_m (M^{-1} s^{-1})
wtMnP	90	256	2.84×10^6	55	253	4.60×10^6
R177A	1.64×10^3	187	0.11×10^6	39	190	4.87×10^6
R177K	2.32×10^3	264	0.11×10^6	44	273	6.20×10^6
E35Q[b]	4.4×10^3	0.77	1.75×10^2			

[a] Reactions were carried out in 50 mM potassium malonate (pH 4.5). Apparent K_m and k_{cat} values for Mn^{II} were determined using 0.2 mM H_2O_2. Apparent K_m and k_{cat} values for H_2O_2 were determined using 5 mM Mn^{II}. [b] From ref *44*.

Table 3: Steady-State Kinetic Parameters for Wild-Type and Mutant MnPs for Ferrocyanide Oxidation[a]

enzyme	K_m (mM)	k_{cat} (s^{-1})	k_{cat}/K_m (M^{-1} s^{-1})
wtMnP	21	38	1.8×10^3
R177A	26	42	1.6×10^3
R177K	16	37	2.2×10^3

[a] Reactions were carried out in 20 mM potassium malonate (pH 4.5). Apparent K_m and k_{cat} values for ferrocyanide were determined using 0.2 mM H_2O_2.

Table 4: Transient-State Kinetic Parameters for MnPI Formation and Reduction

	MnPI formation	MnPI reduction	
enzyme	H_2O_2[a] k_{1app} (M^{-1} s^{-1})	Mn^{II} [a] k_{2app} (M^{-1} s^{-1})	bromide[b] $k_{2'app}$ (M^{-1} s^{-1})
wtMnP	$(6.35 \pm 0.06) \times 10^6$	$\sim 3 \times 10^7$	$(1.15 \pm 0.01) \times 10^3$
R177A	$(5.91 \pm 0.07) \times 10^6$	$(3.41 \pm 0.07) \times 10^6$	$(1.31 \pm 0.01) \times 10^3$
R177K	$(6.13 \pm 0.04) \times 10^6$	$(3.62 \pm 0.03) \times 10^6$	$(1.13 \pm 0.01) \times 10^3$

[a] Reactions were carried out in 50 mM potassium malonate (pH 4.5) (ionic strength of 0.1 M). [b] Reactions were carried out in 20 mM potassium succinate (pH 3.0).

Reduction of MnP Compound I by Mn^{II}. The reduction of MnPI by Mn^{II} was assessed at the optimal pH of 4.5 at a wavelength of 417 nm, the isosbestic point between compound II and native MnP. The observed rate constants for wtMnP with excess Mn^{II} concentrations are too high to measure for Mn^{II} concentrations 30-fold greater than the enzyme concentration. Therefore, the second-order rate constant for wtMnP was estimated to be $\sim 3 \times 10^7$ M^{-1} s^{-1} using low concentrations of Mn^{II}, conditions not obeying strict pseudo-first-order kinetics. In contrast, the k_{2obs} values for mutant MnPI reduction with a 10−50-fold excess of Mn^{II} are measurable and linearly proportional to the Mn^{II} concentrations with a zero intercept, an indication of irreversible, second-order kinetics (data not shown). Second-order rate constants (k_{2app}) for MnPI reduction are shown in Table 4. The k_{2app} values for the Arg177 mutant enzymes are ~10-fold lower than the estimated k_{2app} for wtMnP.

Reduction of MnP Compound I by Bromide. The reduction of wtMnPI by bromide was recently described as a single, two-electron reduction from MnPI to native enzyme (*52*). The reduction of the R177K and R177A compounds I with various concentrations of Br^- was assessed at 407 nm and exhibited single-exponential character. As for wtMnP, the k_{2obs} values were linearly proportional to the Br^- concentra-

Table 5: Kinetic Parameters for the Reduction of MnPI and MnPII by Ferrocyanide and DMP[a]

	ferrocyanide		2,6-dimethoxyphenol	
enzyme	MnPI reduction k_{2app} (M^{-1} s^{-1})	MnPII reduction k_{3app} (M^{-1} s^{-1})	MnPI reduction k_{2app} (M^{-1} s^{-1})	MnPII reduction k_{3app} (M^{-1} s^{-1})
wtMnP	$(1.33 \pm 0.03) \times 10^6$	$(1.80 \pm 0.09) \times 10^3$	$(5.12 \pm 0.07) \times 10^3$	60 ± 6
R177A	$(1.11 \pm 0.01) \times 10^6$	$(1.45 \pm 0.02) \times 10^3$	$(5.61 \pm 0.12) \times 10^3$	60 ± 1.3
R177K	$(2.43 \pm 0.03) \times 10^6$	$(6.63 \pm 0.08) \times 10^3$	$(8.82 \pm 0.10) \times 10^3$	366 ± 39

[a] Reactions were carried out in 20 mM potassium malonate (pH 4.5) (ionic strength of 0.1 M).

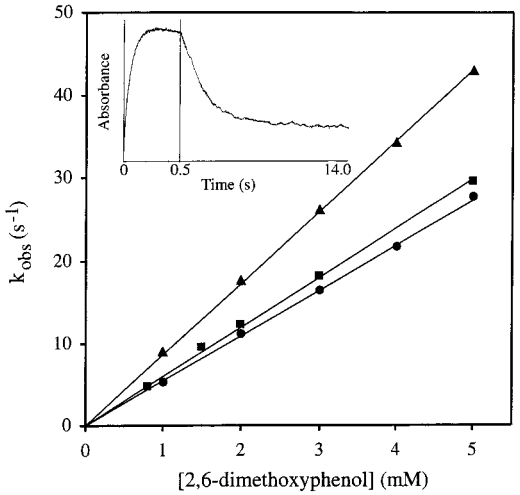

FIGURE 2: Kinetics of MnPI reduction of wtMnP (●) and the R177A (■) and R177K (▲) mutants by DMP in 20 mM potassium malonate (pH 4.5). The inset shows a typical trace at 420 nm of the reduction of 1 μM wild-type MnPI and subsequently of MnPII by DMP.

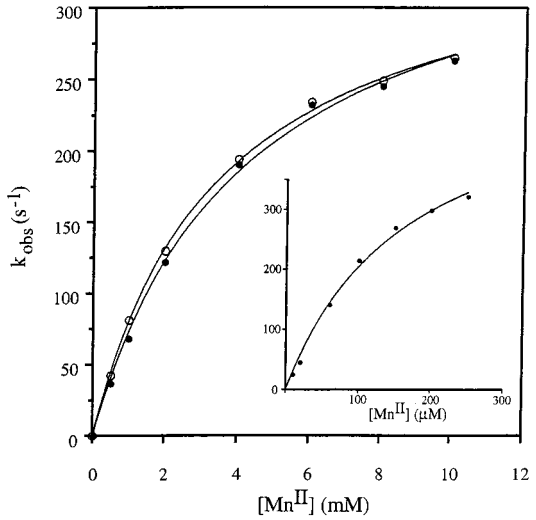

FIGURE 3: Kinetics of compound II reduction of R177A (○) and R177K (●) by Mn^{II} in 20 mM potassium malonate (pH 4.5). The inset shows the kinetics of compound II reduction of wild-type MnP in 20 mM potassium malonate (pH 4.5).

tions with a zero intercept, an indication of irreversible, second-order kinetics. The $k_{2'app}$ values for wtMnP and both mutant MnPs were similar (Table 4).

Reduction of MnP Compounds I and II by Ferrocyanide and 2,6-Dimethoxyphenol. The reduction of MnPI and MnPII by ferrocyanide or DMP was assessed in a two-phase reaction at 420 nm. This is possible because MnPI reduction by these substrates is at least 100-fold faster than MnPII reduction. Exponential traces of MnPI reduction were used to obtain k_{2obs} values, which were linearly dependent on the substrate concentration for both ferrocyanide and DMP (Figure 2). Apparent second-order rate constants, k_{2app}, are listed in Table 5. In contrast to the rates for the reduction of MnPI by Mn^{II}, the k_{2app} values for MnPI reduction by ferrocyanide or DMP were similar for the wild-type and mutant enzymes. The k_{3obs} values for MnPII reduction were also linearly proportional to various ferrocyanide and DMP concentrations used in reactions with both mutant and wtMnP enzymes (data not shown). For ferrocyanide and DMP, the calculated k_{3app} values were similar for wtMnP and R177A MnPs (Table 5). However, for R177K, the apparent rate constants are ~2-fold higher for compound I and II reduction by ferrocyanide and ~6-fold higher for compound II reduction by DMP than those for the wild-type and R177A MnPs.

Reduction of MnP Compound II by Mn^{II}. The MnPII reduction by Mn^{II} is the rate-limiting step in the MnP catalytic cycle (*35*−*38*). The reduction of wild-type and mutant MnP compounds II to native enzyme was followed at 406 nm under pseudo-first-order kinetics, using an excess of Mn^{II}. The plots of the k_{3obs} versus Mn^{II} concentrations leveled off at higher Mn^{II} concentrations (Figure 3). This

Table 6: Kinetic Parameters for the Reduction of MnPII by Mn^{II} [a]

enzyme	k_3 (s^{-1})	K_D (μM)	k_{3app} (M^{-1} s^{-1})
wtMnP	$(5.5 \pm 0.4) \times 10^2$	$(1.7 \pm 0.2) \times 10^2$	3.30×10^6
R177A	$(3.6 \pm 0.06) \times 10^2$	$(3.5 \pm 0.17) \times 10^3$	0.10×10^6
R177K	$(3.8 \pm 0.12) \times 10^2$	$(4.2 \pm 0.3) \times 10^3$	0.09×10^6
E35Q[b]	0.69 ± 0.03	$(8.0 \pm 0.6) \times 10^3$	86.3

[a] Reactions were carried out in 20 mM potassium malonate (pH 4.5) (ionic strength of 0.1 M). [b] From ref *44*.

can be explained by a binding interaction between reactants, according to eqs 1−3:

$$\text{MnPII} + \text{Mn}^{\text{II}} \overset{K_D}{\rightleftharpoons} \text{MnPII}-\text{Mn}^{\text{II}} \xrightarrow{k_3} \text{MnP} + \text{Mn}^{\text{III}} \quad (1)$$

$$k_{3obs} = k_3/(1 + K_D/[\text{Mn}^{\text{II}}]) \quad (2)$$

$$K_D = [\text{MnPI}][\text{Mn}^{\text{II}}]/[\text{MnPII}-\text{Mn}^{\text{II}}] \quad (3)$$

where k_3 is a first-order rate constant (s^{-1}) and K_D is a dissociation constant (M). The calculated values for the first-order rate constant and the dissociation constant are listed in Table 6. Values for the Mn binding site mutant, E35Q, are also listed for comparison. The rate constants k_3 are similar for the wild-type and Arg177 mutant MnPs. In contrast, the dissociation constants, K_D, for the mutant enzymes increased ~20−25-fold. As previously reported (*44*), both the rate constant and binding constant are affected by the E35Q mutant (Table 6). The calculated apparent second-order rate constants, k_3/K_D, for the Arg177 mutant enzymes exhibit a ~30-fold decrease in the rate of reaction.

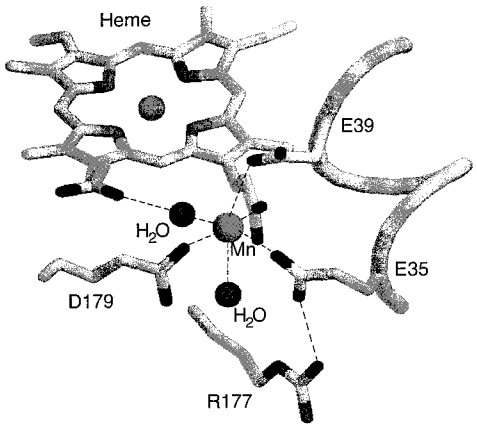

FIGURE 4: Manganese binding site of manganese peroxidase (*26*).

DISCUSSION

Although the catalytic cycle of MnP is similar to that of other fungal and plant peroxidases, this enzyme is unique in that it oxidizes Mn^{II} to Mn^{III} (*3*, *18*, *19*, *33*−*36*). The latter, complexed with an organic acid chelator, diffuses from the enzyme to oxidize the terminal phenolic substrate. The MnP crystal structure (*26*, *54*) indicates there is a cation binding site at the protein surface, consisting of the carboxylates of Asp179, Glu35, Glu39, and heme propionate 6. Mutagenesis studies with the Mn binding ligands, Asp179, Glu35, and Glu39, revealed the role of these ligands in Mn oxidation (*43*, *44*). All the Mn binding site mutants, which eliminated the carboxylic acid functional group, exhibit a significant decrease in the level of Mn binding and in the Mn^{II} oxidation rate. These studies indicate that MnP has a single Mn binding and oxidation site (*43*, *44*, *46*, *54*).

In addition to the Mn ligands, Arg177 has been implicated in Mn binding. The crystal structure shows that Arg177 forms a salt bridge with Glu35, thereby orienting Glu35 for efficient Mn binding (Figure 4) (*26*). Furthermore, deduced amino acid sequence comparisons between several MnP and LiP enzymes from different fungi show that Arg177 is conserved within the MnPs but is replaced by an Ala in the LiPs (*16*).

The *P. chrysosporium* homologous gene expression system (*42*) was used to express mutant genes under the control of the *gpd* gene promoter. Active, heme-containing mutant enzymes were secreted into the extracellular medium and were purified to homogeneity by a combination of chromatographic methods. The R177A and R177K enzymes were essentially identical to wtMnP with respect to chromatographic properties and molecular mass, suggesting that these mutations do not lead to significant conformational alterations of the variant proteins. The optical absorption spectral features of the ferric states and of the oxidized states (MnPI and MnPII) for the R177 variants were essentially identical to those of wtMnP, suggesting that the heme environment of MnP also is not altered significantly by these mutations.

Resonance Raman spectroscopy is well suited for the determination of coordination and spin states of hemes (*55*). In particular, the ν^3 and ν^{10} vibration modes are generally easily identified and, hence, serve as useful indicators. The ν^3 and ν^{10} bands (Figure 1) indicate the coexistence of six-coordinate high-spin and five-coordinate high-spin (6cHS and 5cHS) heme species at room temperature. The mixture of species is consistent with the presence of a six-coordinate heme with water bound in equilibrium with a five-coordinate heme iron lacking a water ligand. In this study and in our previous study of Mn binding site mutants (*44*), the ν^3 mode exhibits a slightly higher 5cHS versus 6cHS ratio for the mutant enzymes than wtMnP. Otherwise, our RR results indicate that the R177K and R177A mutations appear to have little or no effect on the structure and coordination state equilibrium of the heme, suggesting that the mutant proteins are produced without undergoing significant changes in either the overall structure or the heme environment.

In contrast to a negligible effect on spectroscopic properties, mutations at Arg177 significantly alter the kinetic properties of MnP. The apparent K_m values for oxidation of Mn^{II} by the mutant MnPs increase ∼20-fold compared to those of wtMnP, while the turnover numbers (k_{cat}) for the mutant enzymes remain similar to those of wtMnP. These data differ significantly from the kinetic results for the Mn binding site mutants (*44*), where a 50-fold increase in K_m was accompanied by a 300-fold decrease in k_{cat} for the single mutants. This suggests that, unlike the Mn binding ligands, Arg177 is involved in binding of Mn^{II} but apparently not in electron transfer.

Transient-state kinetic analysis of the individual steps in the MnP catalytic cycle shows that these mutations have a significant effect on the reduction of the oxidized intermediates, MnPI and MnPII, by Mn^{II}. The apparent second-order rate constants (k_{2app}) for MnPI reduction in the mutant enzymes are decreased by ∼10-fold compared to those of wtMnP. This second-order constant combines the equilibrium dissociation constant and rate constant; however, we suggest that only the change in binding of Mn^{II} to MnPI contributes to the decrease in k_{2app} with these mutant enzymes, based on steady-state kinetic analysis. The reduction of MnPII, the rate-limiting step in the catalytic cycle, exhibits saturation kinetics for both the wild-type and mutant MnPs. While the equilibrium dissociation constants, K_D, for the Arg177 mutants are ∼22-fold higher than that for wtMnP, the first-order rate constants, k_3, are similar for the wild-type and mutant MnPs. This strongly suggests that the mutations mainly affect the binding of Mn^{II} to the enzyme but have little effect on the rate of electron transfer from the Mn^{II} to the oxidized heme intermediates.

The apparent rate constants for reduction of MnPI and MnPII by substrates apparently not oxidized at the Mn binding site, such as ferrocyanide, 2,6-dimethoxyphenol, and bromide, are similar for the wild-type and mutant MnPs. The K_m and k_{cat} values for the oxidation of ferrocyanide by MnP also are not affected by these mutations, indicating that neither ferrocyanide, phenol (*44*), nor bromide (*52*) oxidation is affected significantly by mutations at the Mn binding site. This suggests that these substrates neither bind nor are oxidized at this site. Furthermore, the mutations at Arg177 affect neither the K_m for H_2O_2 nor the rate of MnPI formation by H_2O_2, suggesting that neither binding nor reduction of H_2O_2 is significantly altered.

Our results indicate that Mn^{II} oxidation by MnP can be separated into at least two steps: the binding of Mn^{II} to the Mn binding site, followed by the electron transfer from Mn^{II} to the oxidized heme. Steady-state and transient-state kinetic experiments indicate that both Arg177 mutations affect the binding of Mn^{II} to the enzyme. The apparent K_m values increase ∼20-fold, and the dissociation constants, K_D, for

MnPII reduction increase ~22-fold for both the R177K and the R177A mutants. In particular, the transient-state kinetic measurements of MnPII reduction show that, while the mutants have a reduced ability to bind Mn^{II}, the first-order rate constants for the reduction of MnPII by Mn^{II} are similar for the wild-type and mutant MnPs, indicating that, once the Mn is bound, electron transfer proceeds efficiently regardless of the mutation at Arg177. Binding of Mn^{II} to the protein results in the hexacoordinate ligation of this metal with the probable lowering of the redox potential for Mn^{II} oxidation. Since the Mn^{II} binding ligands remain unchanged in the Arg177 mutants, the ligation geometry of Mn^{II} in the binding site in the presence of high Mn concentrations probably is unaffected. In fact, the lack of change in the electron-transfer rates for the Arg177 variants suggests a lack of change in the redox potential between the mutant and wild-type enzymes. In contrast, mutation of a Mn ligand such as Asp179, Glu35, or Glu39 has been shown to affect the ligation geometry of the Mn^{II} binding site (*54*) and the electron-transfer rate. Indeed, electron transfer from Mn^{II} to the heme in the E35Q, E39Q, and D179N ligand mutants is much slower than for the wild type (*44*), suggesting that the redox potential of the bound Mn in the latter variants is higher than that of Mn bound to wtMnP.

Crystallographic studies of the Mn ligand mutants suggest that Glu35 and Glu39 assume alternate conformations upon Mn^{II} binding, whereby the side chains of Glu35 and Glu39 swing out toward the protein surface, forming an open configuration in the absence of Mn^{II}, but adapt a closed configuration when Mn^{II} is bound (*54*). The interaction between Arg177 and Glu35 may control this conformational change at the Mn binding site. Crystallographic studies with the D179N mutant (*54*) show that the R177−E35 bond is ~2.81 Å long in the closed (Mn-occupied) structure, while in the open (Mn-unoccupied) structure, the distance increases to ~4.39 Å. Breaking this salt bridge by mutation in R177A and R177K or in E35Q probably affects the ability of the enzyme to adopt the closed conformation upon Mn binding, resulting in an increase in the apparent Mn binding constant. Indeed, the results of this study show that disruption of the salt bridge between Arg177 and Glu35 by mutation of Arg177 results in a decrease in Mn^{II} affinity, indicating that this salt bridge is essential for Mn binding.

Several mutations of the Mn ligand, Glu35, have been reported, including E35Q (*44*) which changes the carboxylate to an amide and E35D (*46*) which shortens the side chain of the ligand without changing the functional carboxylate group. Nevertheless, both mutations significantly affect both the binding of Mn^{II} and the rate of electron transfer from Mn^{II} to the oxidized heme. Since both mutations exhibit a decrease in the rate of electron transfer, the ligation of Mn^{II} in the binding site is likely to be affected. This suggests, as confirmed in the crystal structure, that Arg177 may anchor the position of the carboxylate of Glu35 in the Mn^{II}-occupied closed configuration of the protein. Shortening the side chain of this residue by one methylene in the E35D mutant probably does not affect the salt bridge to Arg177, but it may restrain the carboxylate of this ligand from making a strong bond with the Mn^{II} atom, resulting in a disruption of the ligation for Mn^{II} and hence in the electron-transfer rate as observed (*46*). Crystal structure analysis of these R177 and E35D mutant enzymes should reveal their ligation geometry. Additional studies aimed at examining these possibilities are planned.

REFERENCES

1. Buswell, J. A., and Odier, E. (1987) *CRC Crit. Rev. Biotechnol. 6*, 1−60.
2. Kirk, T. K., and Farrell, R. L. (1987) *Annu. Rev. Microbiol. 41*, 465−505.
3. Gold, M. H., Wariishi, H., and Valli, K. (1989) *ACS Symp. Ser. 389*, 127−140.
4. Bumpus, J. A., and Aust, S. D. (1987) *BioEssays 6*, 166−170.
5. Hammel, K. E. (1989) *Enzyme Microb. Technol. 11*, 776−777.
6. Joshi, D. K., and Gold, M. H. (1993) *Appl. Environ. Microbiol. 59*, 1779−1785.
7. Reddy, G. V. B., Sollewijn Gelpke, M. D., and Gold, M. H. (1998) *J. Bacteriol. 180*, 5159−5164.
8. Kuwahara, M., Glenn, J. K., Morgan, M. A., and Gold, M. H. (1984) *FEBS Lett. 169*, 247−250.
9. Gold, M. H., and Alic, M. (1993) *Microbiol. Rev. 57*, 605−622.
10. Hammel, K. E., Jensen, K. A., Jr., Mozuch, M. D., Landucci, L. L., Tien, M., and Pease, E. A. (1993) *J. Biol. Chem. 268*, 12274−12281.
11. Wariishi, H., Valli, K., and Gold, M. H. (1991) *Biochem. Biophys. Res. Commun. 176*, 269−275.
12. Bao, W., Fukushima, Y., Jensen, K. A., Jr., Moen, M. A., and Hammel, K. E. (1994) *FEBS Lett. 354*, 297−300.
13. Périé, F. H., and Gold, M. H. (1991) *Appl. Environ. Microbiol. 57*, 2240−2245.
14. Orth, A. B., Royse, D. J., and Tien, M. (1993) *Appl. Environ. Microbiol. 59*, 4017−4023.
15. Hatakka, A. (1994) *FEMS Microbiol. Rev. 13*, 125−135.
16. Gold, M. H., Youngs, H. L., and Sollewijn Gelpke, M. D. (1999) in *Metals in Biological Systems* (Sigel, H., and Sigel, A., Ed.) Marcel Dekker, New York (in press).
17. Glenn, J. K., and Gold, M. H. (1985) *Arch. Biochem. Biophys. 242*, 329−341.
18. Glenn, J. K., Akileswaran, L., and Gold, M. H. (1986) *Arch. Biochem. Biophys. 251*, 688−696.
19. Wariishi, H., Valli, K., and Gold, M. H. (1992) *J. Biol. Chem. 267*, 23688−23695.
20. Orth, A. B., Rzhetskaya, M., Cullen, D., and Tien, M. (1994) *Gene 148*, 161−165.
21. Pease, E. A., Andrawis, A., and Tien, M. (1989) *J. Biol. Chem. 264*, 13531−13535.
22. Pribnow, D., Mayfield, M. B., Nipper, V. J., Brown, J. A., and Gold, M. H. (1989) *J. Biol. Chem. 264*, 5036−5040.
23. Mayfield, M. B., Godfrey, B. J., and Gold, M. H. (1994) *Gene 142*, 231−235.
24. Godfrey, B. J., Mayfield, M. B., Brown, J. A., and Gold, M. H. (1990) *Gene 93*, 119−124.
25. Alic, M., Akileswaran, L., and Gold, M. H. (1997) *Biochim. Biophys. Acta 1338*, 1−7.
26. Sundaramoorthy, M., Kishi, K., Gold, M. H., and Poulos, T. L. (1994) *J. Biol. Chem. 269*, 32759−32767.
27. Kunishima, N., Fukuyama, K., Matsubara, H., Hatanaka, H., Shibano, Y., and Amachi, T. (1994) *J. Mol. Biol. 235*, 331−344.
28. Petersen, J. F., Tams, J. W., Vind, J., Svensson, A., Dalboge, H., Welinder, K. G., and Larsen, S. (1993) *J. Mol. Biol. 232*, 989−991.
29. Schuller, D. J., Ban, N., Huystee, R. B., McPherson, A., and Poulos, T. L. (1996) *Structure 4*, 311−321.
30. Edwards, S. L., Raag, R., Wariishi, H., Gold, M. H., and Poulos, T. L. (1993) *Proc. Natl. Acad. Sci. U.S.A. 90*, 750−754.
31. Mino, Y., Wariishi, H., Blackburn, N. J., Loehr, T. M., and Gold, M. H. (1988) *J. Biol. Chem. 263*, 7029−7036.
32. Banci, L., Bertini, I., Pease, E. A., Tien, M., and Turano, P. (1992) *Biochemistry 31*, 10009−10017.

33. Dunford, H. B., and Stillman, J. S. (1976) *Coord. Chem. Rev. 19*, 187−251.
34. Renganathan, V., and Gold, M. H. (1986) *Biochemistry 25*, 1626−1631.
35. Wariishi, H., Akileswaran, L., and Gold, M. H. (1988) *Biochemistry 27*, 5365−5370.
36. Wariishi, H., Dunford, H. B., MacDonald, I. D., and Gold, M. H. (1989) *J. Biol. Chem. 264*, 3335−3340.
37. Kuan, I. C., Johnson, K. A., and Tien, M. (1993) *J. Biol. Chem. 268*, 20064−20070.
38. Kishi, K., Wariishi, H., Marquez, L., Dunford, H. B., and Gold, M. H. (1994) *Biochemistry 33*, 8694−8701.
39. Tuor, U., Wariishi, H., Schoemaker, H. E., and Gold, M. H. (1992) *Biochemistry 31*, 4986−4995.
40. Valli, K., and Gold, M. H. (1991) *J. Bacteriol. 173*, 345−352.
41. Valli, K., Wariishi, H., and Gold, M. H. (1992) *J. Bacteriol. 174*, 2131−2137.
42. Mayfield, M. B., Kishi, K., Alic, M., and Gold, M. H. (1994) *Appl. Environ. Microbiol. 60*, 4303−4309.
43. Kusters-van Someren, M., Kishi, K., Lundell, T., and Gold, M. H. (1995) *Biochemistry 34*, 10620−10627.
44. Kishi, K., Kusters-van Someren, M., Mayfield, M. B., Sun, J., Loehr, T. M., and Gold, M. H. (1996) *Biochemistry 35*, 8986−8994.
45. Kishi, K., Hildebrand, D. P., Kusters-van Someren, M., Gettemy, J., Mauk, A. G., and Gold, M. H. (1997) *Biochemistry 36*, 4268−4277.
46. Whitwam, R. E., Brown, K. R., Musick, M., Natan, M. J., and Tien, M. (1997) *Biochemistry 36*, 9766−9773.
47. Alic, M., Clark, E. K., Kornegay, J. R., and Gold, M. H. (1990) *Curr. Genet. 17*, 305−311.
48. Godfrey, B. J., Akileswaran, L., and Gold, M. H. (1994) *Appl. Environ. Microbiol. 60*, 1353−1358.
49. Alic, M., Letzring, C., and Gold, M. H. (1987) *Appl. Environ. Microbiol. 53*, 1464−1469.
50. Laemmli, U. K. (1970) *Nature 227*, 680−685.
51. Cheddar, G., Meyer, T. E., Cusanovich, M. A., Stout, C. D., and Tollin, G. (1989) *Biochemistry 28*, 6318−6322.
52. Sheng, D., and Gold, M. H. (1997) *Arch. Biochem. Biophys. 345*, 126−134.
53. Alic, M., Mayfield, M. B., Akileswaran, L., and Gold, M. H. (1991) *Curr. Genet. 19*, 491−494.
54. Sundaramoorthy, M., Kishi, K., Gold, M. H., and Poulos, T. L. (1997) *J. Biol. Chem. 272*, 17574−17580.
55. Spiro, T. G. (1988) in *Biological Applications of Raman Spectroscopy*, Wiley, New York.

BI990943C